Acetyl-CoA Synthetase 2 Promotes Acetate Utilization and Maintains Cancer Cell Growth under Metabolic Stress

Zachary T. Schug,[1,8] Barrie Peck,[2,8,11] Dylan T. Jones,[3] Qifeng Zhang,[4] Shaun Grosskurth,[5] Israt S. Alam,[6] Louise M. Goodwin,[5] Elizabeth Smethurst,[4] Susan Mason,[1] Karen Blyth,[1] Lynn McGarry,[1] Daniel James,[1] Emma Shanks,[1] Gabriela Kalna,[1] Rebecca E. Saunders,[2] Ming Jiang,[2] Michael Howell,[2] Francois Lassailly,[2] May Zaw Thin,[2] Bradley Spencer-Dene,[2] Gordon Stamp,[2] Niels J.F. van den Broek,[1] Gillian Mackay,[1] Vinay Bulusu,[7] Jurre J. Kamphorst,[7] Saverio Tardito,[1] David Strachan,[1] Adrian L. Harris,[3] Eric O. Aboagye,[6] Susan E. Critchlow,[5] Michael J.O. Wakelam,[4] Almut Schulze,[2,9,10] and Eyal Gottlieb[1,*]

[1]Cancer Research UK, Beatson Institute, Garscube Estate, Switchback Road, Glasgow G61 1BD, UK
[2]Cancer Research UK, London Institute, 44 Lincoln's Inn Fields, London WC2A 3LY, UK
[3]Molecular Oncology Laboratories, Weatherall Institute of Molecular Medicine, University of Oxford, John Radcliffe Hospital, Oxford OX3 9DS, UK
[4]Babraham Institute, Babraham Research Campus, Cambridge CB22 3AT, UK
[5]AstraZeneca, Mereside, Alderley Park, Macclesfield SK10 4TG, UK
[6]Department of Surgery and Cancer, Imperial College London, Hammersmith Hospital, Du Cane Road, London W12 0NN, UK
[7]Institute of Cancer Sciences, University of Glasgow, Garscube Estate, Switchback Road, Glasgow G61 1BD, UK
[8]Co-first author
[9]Present address: Theodor Boveri Institute, Biocenter, University of Würzburg, Am Hubland, 97074 Würzburg, Germany
[10]Present Address: Comprehensive Cancer Center Mainfranken, Josef-Schneider-Strasse 6, 97080 Würzburg, Germany
[11]Present address: The Breakthrough Breast Cancer Research Centre, The Institute of Cancer Research, London SW3 6JB, UK
*Correspondence: e.gottlieb@beatson.gla.ac.uk
http://dx.doi.org/10.1016/j.ccell.2014.12.002

SUMMARY

A functional genomics study revealed that the activity of acetyl-CoA synthetase 2 (ACSS2) contributes to cancer cell growth under low-oxygen and lipid-depleted conditions. Comparative metabolomics and lipidomics demonstrated that acetate is used as a nutritional source by cancer cells in an ACSS2-dependent manner, and supplied a significant fraction of the carbon within the fatty acid and phospholipid pools. ACSS2 expression is upregulated under metabolically stressed conditions and ACSS2 silencing reduced the growth of tumor xenografts. *ACSS2* exhibits copy-number gain in human breast tumors, and ACSS2 expression correlates with disease progression. These results signify a critical role for acetate consumption in the production of lipid biomass within the harsh tumor microenvironment.

INTRODUCTION

Under typical cell culture conditions and in many tissues within the human body, the primary source of lipids for membrane biogenesis is the plasma. However, exposure to lipid-deplete conditions causes a highly coordinated reorganization of the lipid metabolism machinery that is primarily orchestrated by the sterol regulatory element-binding protein (SREBF) family of transcription factors, which drive the expression of genes encoding for enzymes involved in fatty acid and cholesterol biosynthesis. Deregulated expression of many of these metabolic enzymes is a feature of different disease states, including cancer. Importantly, de novo lipogenesis is a key component of anabolic metabolism and is necessary to meet the demands

Significance

Tumors are situated in a metabolically challenging environment where blood supply, and the supply of oxygen and other nutrients that come with it, is scarce. We found that nearly 40% of invasive ductal carcinoma have high expression of acetyl-CoA synthetase 2 (ACSS2). ACSS2, an enzyme that converts acetate to acetyl-CoA, imparts a competitive growth advantage under conditions of metabolic stress by enhancing the ability of cancer cells to use acetate as an additional nutritional source when other carbon sources are scarce or cannot be used to sustain lipid biomass production. This study also identified ACSS2 as a potential molecular target for managing cancer growth.

for biomass production required for growth and survival under unfavorable conditions (Baenke et al., 2013).

Despite knowledge of the relationship between tumor progression and changes in lipid metabolism (Menendez and Lupu, 2007), it was not until the early 1990s that fatty acid synthase (FASN) was strongly associated with recurrence, metastases, and death in breast cancer patients (Kuhajda et al., 1994). Subsequently, de novo fatty acid synthesis was found to be a critical regulator of breast, prostate, and lung cancer growth (Alli et al., 2005; Orita et al., 2008; Pizer et al., 1996a, 1996b, 1996c, 2001; Puig et al., 2009; Zhan et al., 2008). Selective activation of the fatty-acid-synthesis pathway commonly occurs in many cancer types, and, in particular, FASN upregulation was identified as an early event during the development of prostate cancer (Swinnen et al., 2000b, 2002); evidence suggested that this lipogenic phenotype was driven by SREBF signaling (Swinnen et al., 2000a). Furthermore, RNAi silencing of FASN expression in an androgen-receptor-positive prostate cancer cell line strongly inhibited cell proliferation (De Schrijver et al., 2003). It has even been suggested that FASN itself can be sufficient to drive the transformation of prostate cells and may be a good target for antineoplastic therapy (Migita et al., 2009). Consequently, FASN has been the subject of drug development efforts, and specific FASN inhibitors, such as C75 and GSK837149A, have been developed and shown to kill cancer cells as well as synergize with established therapies (Menendez and Lupu, 2007). But crucially, these compounds have been shown to have poor pharmacokinetics or exhibit target-related toxicities. These findings support the hypothesis that targeting lipid synthesis can have a marked effect on cancer growth, but that the current selected targets may not be optimal, highlighting the need for the discovery of additional therapeutic targets that inhibit lipid metabolism.

The sole carbon source and precursor for both fatty acid and cholesterol biosynthesis in mammalian cells is acetyl-CoA. The cytosolic pool of acetyl-CoA is mainly supplied by two different ATP-dependent reactions: cleavage of citrate into oxaloacetate and acetyl-CoA by ATP citrate lyase (ACLY) or the ligation of acetate and CoA by acetyl-CoA synthetase (ACSS). It has been shown that ACLY is required for cell growth and cancer cell survival, and there has been interest in the development of ACLY inhibitors, with some showing potential at inhibiting tumor growth (Beckers et al., 2007; Hatzivassiliou et al., 2005; Zu et al., 2012). However, only a few studies have addressed the potential role of acetate in the context of cancer (Yoshii et al., 2009a, 2009b; Yoshimoto et al., 2001; Yun et al., 2009). There are three genes that encode ACSS proteins, namely *ACSS1*, *ACSS2*, and a more recently proposed third family member *ACSS3* (Luong et al., 2000; Watkins et al., 2007). ACSSs were originally identified as SREBF target genes, but relatively little is known regarding the regulation of ACSS gene expression (Luong et al., 2000; Schwer et al., 2006; Sone et al., 2002). Early studies indicated that ACSS activity controlled acetate uptake (Luong et al., 2000; Tucek, 1967). Herein, we attempted to identify lipid metabolism genes that were critical to the growth and survival of breast and prostate cancer cells in metabolically stressed conditions, such as hypoxia and low lipid availability.

RESULTS

Exposure to Hypoxia and Low Serum Alters Lipid Metabolism

It is now widely accepted that de novo lipogenesis is critical to tumor progression and survival and is driven by the increased expression of a host of lipogenic enzymes (reviewed by Menendez and Lupu, 2007; Zaidi et al., 2013). We initially characterized the dependency of breast cancer cell lines on de novo fatty acid synthesis under high- and low-serum conditions. The FASN inhibitor C75 had no effect on breast cancer cell lines when cultured in the presence of 10% serum (Figure 1A). However, treatment in low serum reduced cell number in the majority of the breast cancer cell lines tested. In addition, the IC_{50} for a recently developed FASN inhibitor, AZ22, was drastically improved when cells were cultured in low serum (Figure 1B and Figure S1A available online).

To delineate changes in the lipid profiles of normoxic versus hypoxic cancer cells, we performed high-resolution acyl chain profiling of phosphatidylcholine (PC) and phosphatidylethanolamine (PE) using liquid chromatography-tandem mass spectrometry (LC-MS/MS)-based lipidomics. We noted a shift in the profile of PC and PE that was mainly characterized by the presence of shorter, more saturated acyl chains in hypoxia compared to normoxia (Figures 1C and S1B). This type of shift is indicative of increased de novo fatty acid synthesis and elongation, which produce mainly saturated fatty acyl-CoA and, to a lesser degree, monounsaturated acyl-CoA (Hilvo et al., 2011; Rysman et al., 2010; Sahar et al., 2014). Since glucose can contribute to the synthesis of phospholipids by supplying the glycerol backbone via glycerol 3-phosphate and also by the production of the fatty acid precursor acetyl-CoA, we traced the fate of $^{13}C_6$-glucose using targeted metabolomics and lipidomics (Figure S1C). It should be noted that all metabolomics experiments throughout the entire study used custom-formulated serum-like tissue culture medium (SMEM) containing concentrations of metabolites more physiologically relevant to human plasma than what is typically found in standard growth mediums. Selected metabolite concentrations were based on the most current literature where available and also as defined by the NIH (http://www.nlm.nih.gov/medlineplus/ency/article/003361.htm; Table S1).

A high volume of medium to cell number ratio was maintained to ensure cells were exposed to concentrations of metabolites that were still within the reported physiological ranges. For instance, we found that 20% of available glucose in normoxia and 40% during hypoxia was consumed during a typical 24 hr incubation (Figure S1D). We also noted that, in normoxia, glucose was readily used by the tricarboxylic acid (TCA) cycle with >75% of citrate labeled from glucose; however, under hypoxic conditions, this contribution was decreased 5-fold (Figure S1E). This was likely due to the well-characterized inactivation of pyruvate dehydrogenase by pyruvate dehydrogenase kinase 1 under hypoxic conditions (Kim et al., 2006; Papandreou et al., 2006). In addition, an in-depth analysis of the most abundant PC species (34:1) detected a high degree of labeling under normoxic conditions (>95%), suggesting that the majority of PC(34:1) had been synthesized de novo from glucose (Figure S1F). Strikingly, in hypoxia, there was a sharp decline in the labeling of the fatty acid component of PC(34:1) (i.e., isotopologs $\geq$ M+4), but not
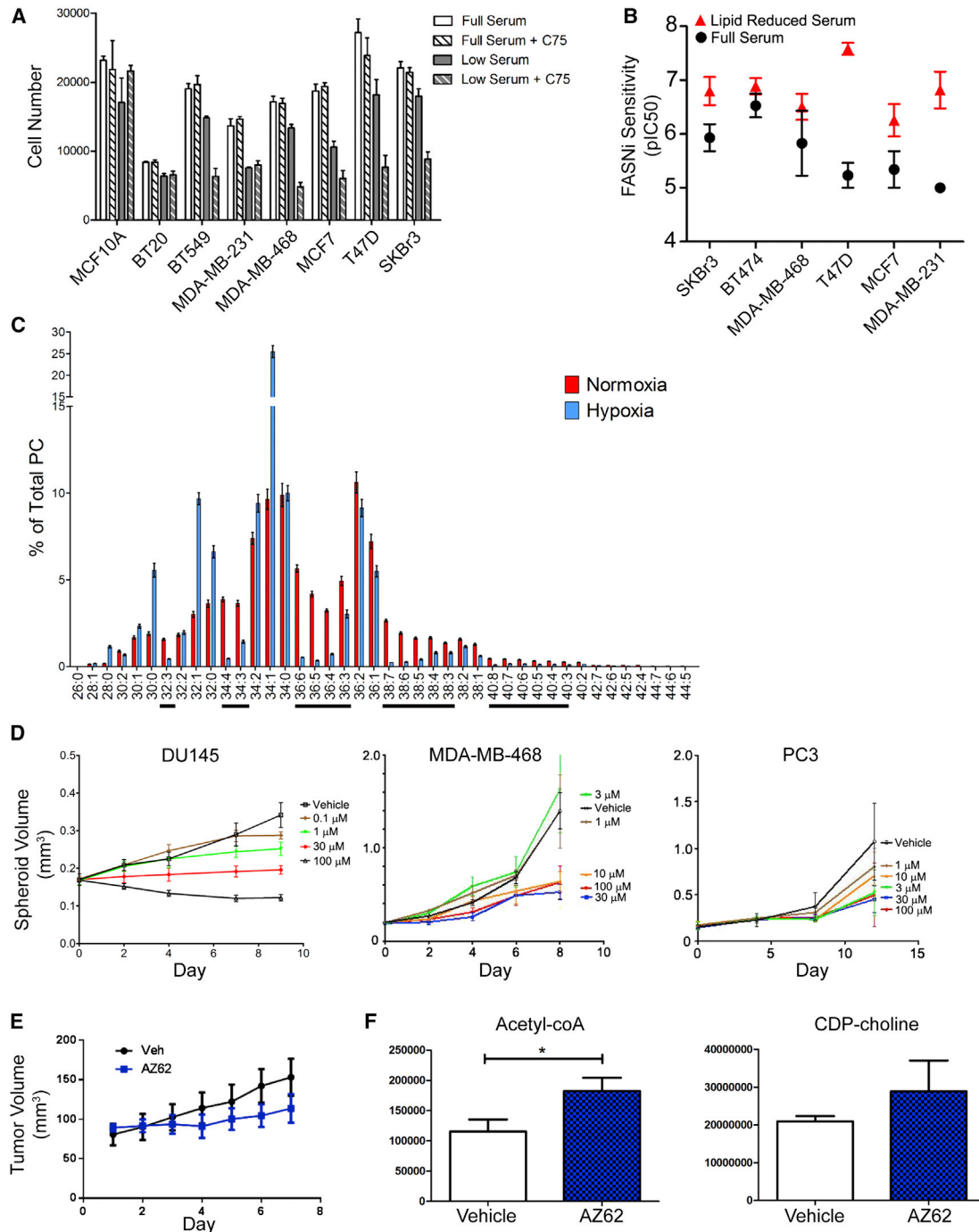
Figure 1. In Vivo Conditions Are Most Closely Mimicked by Culturing Cells in Low Serum and Hypoxia

(A) Sensitivity of breast cancer cells to C75 (2.5 μM) treatment in high (10%) and low (1%) serum concentrations. Data are presented as mean ± SEM (n = 3).

(B) pIC$_{50}$ (−log IC$_{50}$) values for AZ22 in breast cancer cell lines cultured in full serum or lipid-reduced serum. Data are presented as mean ± SEM (n ≥ 3).

(C) Lipid profiling of PC by LC-MS under normoxic (21%) and hypoxic (0.1%) conditions in MDA-MB-468 breast cancer cells grown in low serum. PC species containing highly polyunsaturated acyl chains (≥3 C = C bonds) are underlined. Data are presented as mean ± SEM (n = 3).

(D) DU145, MDA-MB-468, and PC3 spheroids were grown in full medium and in the presence of AZ22 for 8–12 days to determine the dependency of spheroid growth on de novo fatty acid synthesis. Data are presented as mean ± SEM (n ≥ 3).

(E) Short-term tumor xenograft growth of BT474 cells treated with vehicle or AZ62. Tumors were grown to 100 mm^3 and size-matched animals were randomized to AZ62 or vehicle treatment. Animals were treated with AZ62 at 100 mg/kg (oral administration) daily for 7 days. Data are presented as mean ± SEM (n = 4 per group).

(F) Steady-state levels of acetyl-CoA and CDP-choline in BT474 tumor extracts as determined by LC-MS-based metabolomics. Data are presented as mean ± SEM (n = 6 per group).

See also Figure S1 and Table S1.
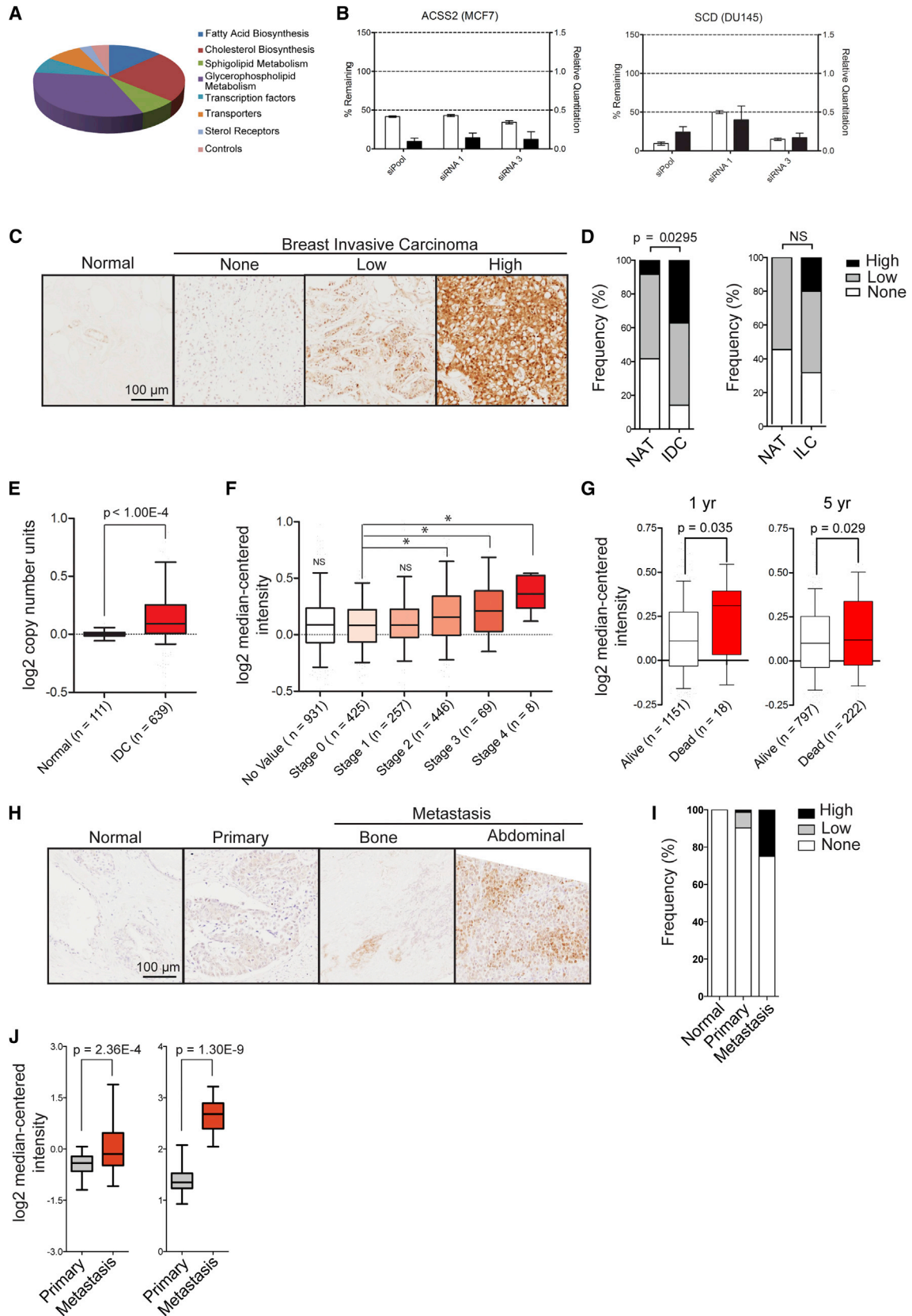
the labeling of the glycerol backbone (M+3) (Figure S1F). These results imply that the majority of glycerol within the PC fraction is generated de novo by the cells, and suggest a strong dependency on biosynthetic pathways (Brockmöller et al., 2012).

Given the observed changes in lipid metabolism and increased sensitivity to FASN inhibition in hypoxia and low serum, we next examined whether spheroids and tumor xenografts, models that naturally generate oxygen and nutrient gradients, also were susceptible to FASN inhibition. DU145, MDA-MB-468, and PC3 spheroid cultures treated with AZ22 were all dose-dependently sensitive to FASN inhibition (Figure 1D). Furthermore, using a different FASN inhibitor (AZ62) with improved pharmacokinetics and increased tolerance in vivo, we found that AZ62 inhibited BT474 xenograft tumor growth (Figures 1E and S1G). Analysis of metabolite extracts from the AZ62-treated tumors by liquid chromatography-mass spectrometry (LC-MS) detected elevated levels of the fatty acid precursor acetyl-CoA and the PC precursor CDP-choline (Figure 1F).

Altogether, these results indicate that metabolic stress induces major changes in the lipid metabolism landscape of cancer cells, creating a dependence on de novo lipogenesis for survival in hypoxia/low serum (Ackerman and Simon, 2014; Bensaad et al., 2014). The data imply that, despite a high level of de novo lipogenesis under hypoxia (30%–50% labeled from glucose via glycerol 3-phosphate), glucose contribution to fatty acid biosynthesis is markedly decreased and an alternative carbon source would be required. Lastly, the growth inhibition observed in conditions of metabolic stress was recapitulated in spheroids and tumors, suggesting that tumors are indeed subject to conditions in which oxygen and lipids are severely limited.

Functional Genomics Identifies *ACSS2* as a Critical Gene for Cancer Cell Survival under Hypoxic or Low-Serum Conditions

Expression of many genes involved in lipid biosynthesis is induced in response to activation of SREBF by the PI3K/Akt/mTORC1-signaling axis (Porstmann et al., 2008), which is frequently deregulated in human cancer. Furthermore, 50% of genes predicted to be highly significant for increasing the biomass of cancer cells by a genome-scale metabolic model of cancer were associated with lipid metabolism (Folger et al., 2011). Based on these independent lines of evidence, we assembled a small interfering RNA (siRNA) library of 66 potential targets with gene ontologies associated with lipid metabolism (Figure 2A; Tables S2 and S3). Functional genomics screens were performed using eight breast and three prostate cancer cell lines (Table S4). Based on our preliminary results with FASN inhibitors (Figure 1), we investigated growth inhibition during metabolic stress: 1% serum in normoxia, 10% serum in hypoxia, and 1% serum in hypoxia compared to the nutrient- and oxygen-rich conditions of 10% serum in normoxia. A strictly standardized mean difference (SSMD) was used to evaluate the potency and selectivity of silencing on growth relative to an internal nontargeting control (Zhang, 2011; Table S4). This preliminary filter was used to rank targets according to the difference in growth inhibition when comparing normoxia to hypoxia or 10% serum to 1% serum conditions (Table S4). The top targets from the screen were reassessed using a different pool of siRNAs (Figure 2B; Table S4). Following siRNA pool deconvolution of all the shortlisted targets, we found the top hits for hypoxia and low serum were, respectively, acetyl-CoA synthetase 2 (ACSS2) and stearoyl-CoA desaturase (SCD) (Figure 2B).

We next performed a comprehensive data mining analysis of the expression and disease association of the targets that passed deconvolution. *ACSS2* had the highest frequency of DNA copy-number gain in breast tumors and was associated with increased ACSS2 expression (Figures S2A and S2B). The relatively focal *ACSS2* amplicon, which contains 47 other genes, spans most of the genomic region encompassing 20q11.22 and does not include any cancer consensus genes (Figures S2C and S2D). In support of the expression data from publically available patient data sets, immunohistochemical staining of tumor microarrays revealed high ACSS2 expression in nearly 40% of invasive ductal carcinomas (IDCs) compared to their normal adjacent tissue samples, with a similar trend observed in invasive lobular carcinomas (ILCs) (Figures 2C and 2D). Focused data mining of a separate breast cancer database noted a significant increase in *ACSS2* copy number in cancer versus normal tissue (Figure 2E; Curtis et al., 2012). There was also a strong correlation between ACSS2 expression and disease progression (Figure 2F; Curtis et al., 2012). A Dunnet's multiple comparison test between stage

Figure 2. ACSS2 Is Frequently Upregulated in Cancer and Positively Correlates with Disease Progression and Poor Survival
(A) Proportional phenotypic classification of siRNA target genes.
(B) Top hits from screening under metabolic stress. Growth data are presented as mean ± SD (white bars, left y axis) and mRNA expression data are presented as mean ± upper and lower limits (n = 3) (black bars, right y axis) and are normalized to a nontargeting control siRNA pool.
(C) Representative immunohistochemistry images of ACSS2 expression from a tissue microarray of breast cancer samples.
(D) Histograms illustrating ACSS2 expression in normal adjacent breast tissue (NAT, n = 12) and (left) IDC (p value = 0.0295; n = 78) and (right) ILC (NS = not significant; n = 75).
(E) *ACSS2* DNA copy-number variation comparing normal and IDC samples (p value = 1.0×10^{-4}, unpaired, two-tailed t test). Boxes represent the upper and lower quartiles, the band represents the median, and the whiskers represent 5–95th percentile.
(F) ACSS2 mRNA expression at different stages of IDC (asterisk, $p < 0.05$, Dunnet multiple comparison test). Boxes represent the upper and lower quartiles, the band represents the median, and the whiskers represent 5–95th percentile.
(G) ACSS2 mRNA expression in invasive carcinoma and the patient survival status at 1 and 5 years (Mann-Whitney test, p values are as indicated). Boxes represent the upper and lower quartiles, the band represents the median, and the whiskers represent 10th–90th percentile.
(H) Representative immunohistochemistry images of ACSS2 expression from a tissue microarray of prostate cancer samples.
(I) Histogram illustrating ACSS2 expression in normal tissue and primary and metastatic prostate cancers.
(J) The p values and fold change showing increased ACSS2 expression in metastatic prostate cancer compared with primary site tumors. Data were obtained from the Grasso (left) and Chandra (right) prostate cancer data sets available from Oncomine. Boxes represent the upper and lower quartiles, the band represents the median, and the whiskers represent minimum and maximum (p values are indicated, unpaired, two-tailed t test).
See also Figure S2 and Tables S2, S3, and S4.
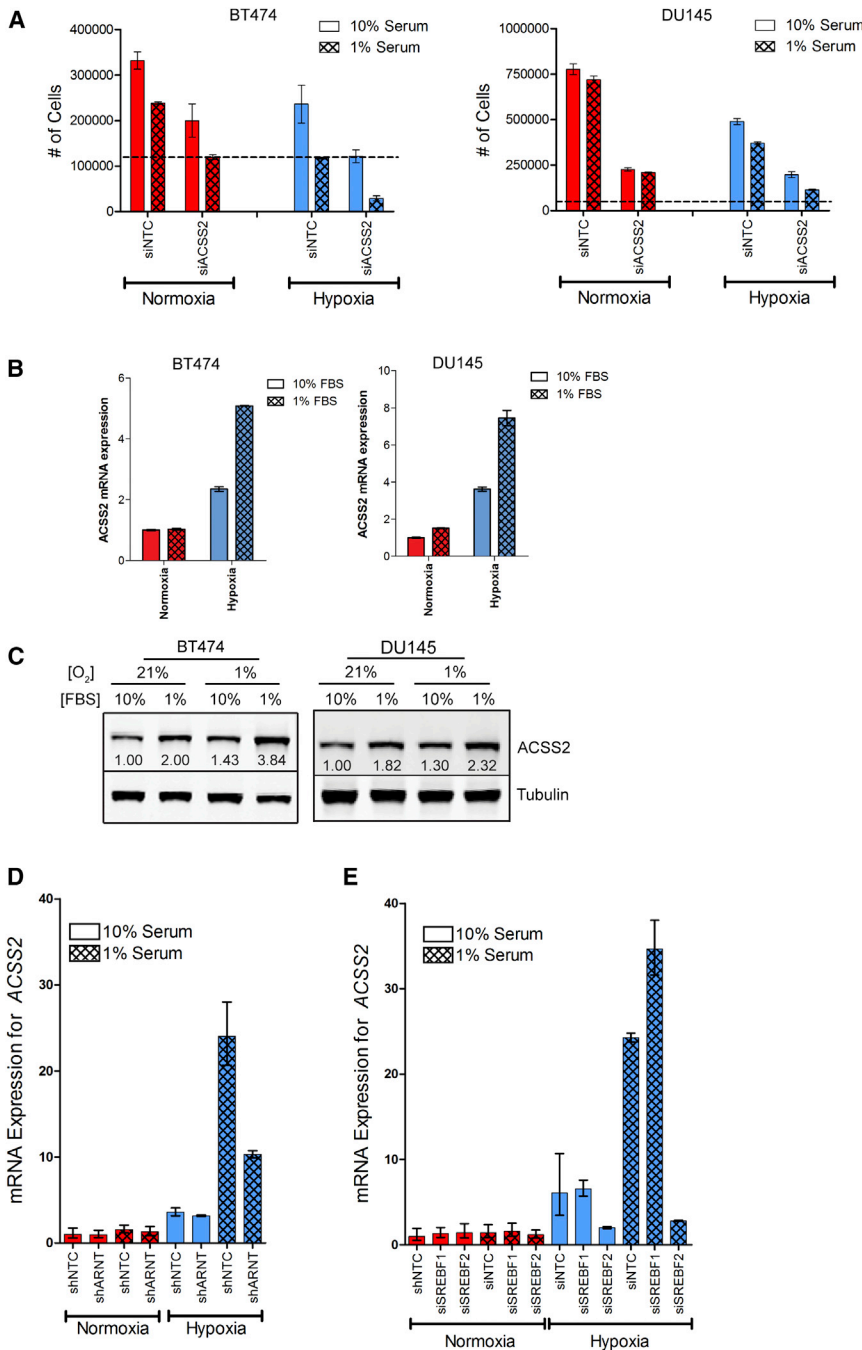
Figure 3. Metabolic Stress Induces Upregulation of ACSS2 and Causes Cells to Become Increasingly Sensitive to ACSS2 Depletion

(A) BT474 and DU145 cell counts at 96 hr post-siRNA transfection. Dotted line represents the seeding density. Data are presented as mean ± SD (n = 3).

(B) ACSS2 mRNA expression in BT474 and DU145 cells under metabolic stress (hypoxia = 0.1% O_2). Error bars represent SEM (n = 2).

(C) ACSS2 protein expression in BT474 and DU145 cells under metabolic stress.

(D) ACSS2 mRNA expression in BT474c1 cells expressing an shRNA against ARNT. Data are normalized to expression of shNTC in normoxia + 10% serum. Error bars represent SEM (n = 3).

(E) ACSS2 mRNA expression in BT474c1 cells transfected with a nontargeting control siRNA or a pool of siRNAs against SREBF1 or SREBF2. Data are normalized to expression of siNTC in 10% serum and normoxia (hypoxia = 0.1% O_2). Error bars represent SEM (n = 3).

See also Figure S3.

data sets, suggesting that ACSS2 may be particularly important in more aggressive prostate cancers and metastases (Figure 2J).

Hypoxia and Low-Serum Culture Conditions Synergistically Enhance ACSS2 Expression

The Cancer Cell Line Encyclopedia was used to identify breast cancer cell lines with strong evidence for *ACSS2* copy-number gain and upregulation (Barretina et al., 2012; Forbes et al., 2011; Shao et al., 2013). Two of the cancer cell lines used in the functional screen had high ACSS2 expression, namely MDA-MB-468 and SKBr3, while BT474 had the overall highest level of DNA copy-number gain and expression (Figures S3A and S3B). DNA copy-number gain for both the 20q arm and 20q11 chromosomal band, containing *ACSS2*, has been reported previously for BT474 and SKBr3, as detected by fluorescence in situ hybridization, genomic hybridization, and comparative genomic hybridization array (Brinkmann et al., 1996; Guan et al., 1996; Pinkel et al., 1998; Rondón-Lagos et al., 2014). Given the enhanced growth inhibition observed by ACSS2 silencing during the functional screening in hypoxia, we measured ACSS2-dependent growth during metabolic stress. Silencing of ACSS2 was most effective at growth inhibition under metabolic stress and, interestingly, was cytotoxic to BT474 cells (Figures 3A and S3C). Furthermore, expression analysis of our panel of cancer cell lines revealed consistent upregulation of ACSS2 at both the mRNA (Figures 3B, S3D, and S3E) and protein levels

0 and all other stages found there was significant upregulation of ACSS2 in stages 2, 3, and 4, and a test of linear trend further confirmed a systematic increase in ACSS2 expression with escalating tumor stage (p = 0.0001) (Figure 2F). Using this same data set, we further noted that ACSS2 expression was significantly higher (p < 0.05; Mann-Whitney test) in patients who did not survive past 1 or 5 years postdiagnosis (Figure 2G). In prostate cancer patients, there was an increased expression of ACSS2 in metastasis compared to primary tumor or normal tissue (Figures 2H and 2I). These results were consistent with observations from two different publically available prostate cancer

(Figure 3C) under metabolic stress. These results reinforced the hypothesis that ACSS2 becomes important for cell proliferation under metabolic stress and that cancer cells harboring *ACSS2* copy-number gains may be more vulnerable to ACSS2 depletion.

A test for mutual exclusivity among 962 breast cancer samples (The Cancer Genome Atlas) revealed a significant tendency toward co-occurrence between ACSS2 and hypoxia-inducible transcription factor (HIF) targets LDHA and PDK1, suggesting it may be a HIF target (Figure S3F). Indeed, small hairpin RNA (shRNA)-mediated silencing of ARNT expression reduced the upregulation of ACSS2 by 2.5-fold (Figures 3D and S3G). However, unlike the complete loss of hypoxia-induced upregulation of LDHA and PDK1 noted after ARNT silencing, some ACSS2 upregulation persisted (Figures 3D and S3H). Since ACSS2 is known to be a target of SREBF signaling (Luong et al., 2000) and SREBFs are activated by lipid depletion (Briggs et al., 1993; Wang et al., 1993), it seemed likely that ACSS2 expression would be controlled by SREBFs. Silencing of SREBF2, but not SREBF1, completely eliminated the upregulation of ACSS2 under conditions of metabolic stress (Figures 3E and S3I). Together, the expression data imply that SREBF2 mainly controls ACSS2 expression, but that ARNT-dependent HIF signaling enhances the upregulation of ACSS2 by SREBF2. Interestingly, the expression of FASN was highly upregulated under metabolic stress and controlled in exactly the same manner as ACSS2, suggesting the two targets are intimately linked (Figure S3J).

Acetate Supports Biosynthesis of Membrane Phospholipids

The molecular function of ACSS2 is to ligate acetate with coenzyme A in an ATP-dependent reaction to produce acetyl-CoA, a metabolite central to a range of cellular processes (Figure 4A). We investigated if acetate contributed to the acetyl-CoA pool and, furthermore, if it was used for lipid synthesis. To that end, BT474c1, a more tumorigenic subclone of BT474, was used. BT474c1 cells, which express similar levels of ACSS2 as their parental cells (Figure S3B), had increased $^{14}C_2$-acetate uptake under hypoxic conditions (Figure 4B). Also, $^{14}C_2$-acetate-dependent fatty acid synthesis increased during metabolic stress (Figure 4C). However, in all cell lines tested, the steady-state levels of acetyl-CoA were much lower in hypoxia (Figure 4D).

To investigate this further, we traced the incorporation of $^{13}C_2$-acetate into the acetyl-CoA pool and found that, at most, 10% was labeled during normoxic and lipid-replete growth conditions, while during metabolic stress, over 50% of the acetyl-CoA pool was labeled by acetate over a 12 hr period (Figure 4E). The mutual mRNA regulation of ACSS2 and FASN suggested acetate was being used to support membrane phospholipid biosynthesis during metabolic stress. To study this, we employed LC-MS/MS-based lipidomics to trace the incorporation of $^{13}C_2$-acetate into the PC(34:1) during metabolic stress. There was a rightward shift of the PC-isotopolog-labeling pattern, indicating that a higher percentage of PC carbon was sourced from acetate during metabolic stress than normal growth conditions (Figure 4F). This shift is highly indicative of an increased availability of acetate-derived acetyl-CoA for fatty acid synthesis, and, importantly, shows that acetate can be a major nutritional source.

ACSS2 Controls Acetate Uptake and Contribution to Fatty Acids

Previous reports had suggested that acetate consumption is dictated by functional expression of ACSS2 (Luong et al., 2000; Tucek, 1967). Measurement of [^{3}H]-acetate uptake in BT474c1 cells, as well as DU145 prostate cancer cells, demonstrated reduced acetate consumption after ACSS2 depletion (Figures 5A and 5B). Interestingly, BT474c1 cells that expressed high levels of ACSS2 exhibited almost twice as much acetate uptake compared to DU145 cells that expressed low levels of ACSS2 (Figures 5B and S3B). We further investigated for signs of inhibition of lipid synthesis by quantifying the substrate of the final enzymatic reaction in the synthesis of PC and PE (Figure 5C). Similar to the results using FASN inhibitors (Figure 1F), CDP-choline and CDP-ethanolamine steady-state levels were elevated upon ACSS2 silencing, suggesting impairment of de novo lipogenesis (Figure 5D). Since serum is a source of lipids, growth factors, and other nutrients, we reassessed ACSS2-dependent growth in lipid-depleted serum (LPDS) to ascertain if the observed growth effects during hypoxia, such as seen in Figure 3, were due to the loss of extracellular lipids or another component in the serum. Cells grown in 10% LPDS were more sensitive to ACSS2 silencing than cells grown in 10% full serum in hypoxia (Figure 5E). Similar to 1% serum, 10% LPDS also induced ACSS2 expression in hypoxia (Figure 5F).

The most highly characterized pathway of acetate metabolism concerns the conversion of acetate to acetyl-CoA and the use of 2-carbon acetyl units to synthesize fatty acids through successive rounds of condensation by FASN (Roncari, 1974, 1975). We investigated if acetate was being used as an anabolic precursor for de novo fatty acid synthesis. The concentration of plasma acetate in humans varies between 0.05 and 0.25 mM (Scheppach et al., 1991; Skutches et al., 1979; Tollinger et al., 1979), but can increase up to 1 mM after alcohol consumption (Lundquist et al., 1962; Tsukamoto et al., 1989). The acetate concentration in mouse and rat plasma ranges between 0.20 and 0.30 mM (Kimura et al., 2013; Maxwell et al., 2010). The acetate concentration in media + 10% serum was measured by gas chromatography-mass spectrometry and determined to be 0.10 mM (Table S1). Besides exogenous sources, acetate can be produced endogenously via protein deacetylation. However, we and others observed that histone acetylation is induced under hypoxia indicating that deacetylation is unlikely an acetate source during metabolically stressed conditions (Vaapil et al., 2012; Watson et al., 2009; our unpublished observations).

Initially, we characterized the contribution of $^{13}C_2$-acetate to fatty acid synthesis by comparing the isotopolog-labeling pattern of palmitate and stearate during metabolic stress. LC-MS-based analysis of palmitate revealed small dose-dependent differences in acetate-dependent palmitate synthesis as the concentration of acetate increased from 0.10 to 0.50 mM (Figure 5G). Similar to the PC-isotopolog-labeling pattern in Figure 4, there was an overall shift in the abundance of isotopologs < M+8 to ≥ M+8 when cells were exposed to metabolic stress, suggesting increased availability of acetate-derived acetyl-CoA for fatty acid synthesis (Figure 5G). Similar results were obtained for stearate (Figure S4A). In addition, silencing of ACSS2 strongly impaired both palmitate and stearate labeling from acetate (Figures S4B and S4C).
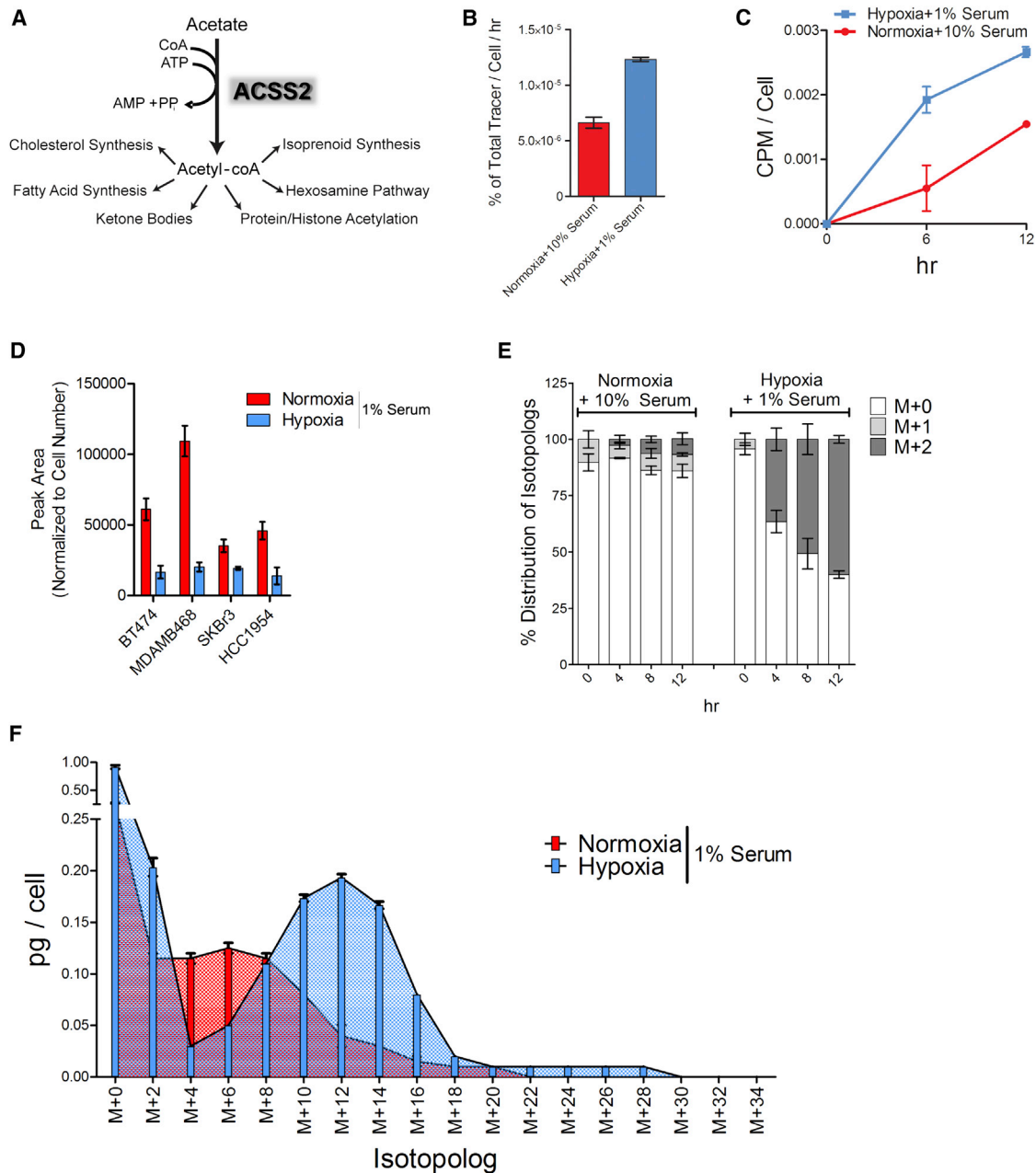
Figure 4. Metabolic Stress Increases Acetate Uptake and Supports Biosynthesis of Membrane Phospholipids

(A) Schematic for the ACSS2 reaction and destinations for nucleocytosolic acetyl-CoA.

(B) $^{14}C_2$-acetate uptake under metabolic stress. Data are presented as mean ± SEM (n = 3).

(C) $^{14}C_2$-acetate-dependent lipid synthesis over a 12 hr period under metabolic stress. Data are presented as mean ± SEM (n = 3).

(D) Steady-state acetyl-CoA levels in a panel of breast cancer cell lines. Data are presented as mean ± SD (n ≥ 3).

(E) Enrichment of 0.20 mM $^{13}C_2$-acetate in the acetyl-CoA pool in BT474c1 cells cultured in normoxia and SMEM + 10% serum or hypoxia and SMEM + 1% serum over a 12 hr period. Data are presented as mean ± SEM (n ≥ 3).

(F) Abundance of PC(34:1) isotopologs in BT474 cells cultured in SMEM + 1% serum supplemented with 0.50 mM $^{13}C_2$-acetate. Area under the curve is shown to highlight the shift in the isotopolog-labeling pattern induced by metabolic stress. Data are presented as mean ± SEM (n ≥ 2).

We next traced the fate of $^{13}C_2$-acetate within the TCA cycle by looking at the isotopolog-labeling pattern of citrate. However, this would be controlled mainly by the other ACSS isoform, ACSS1, which has been shown to be localized to the mitochondria (Fujino et al., 2001). ACSS1 activity did slightly compensate for silencing of ACSS2 under normoxic conditions, in which an active TCA cycle was still running (Figure S4D). This was shown by the increase in M+2 and M+3 labeling of citrate following ACSS2 silencing in normoxia (Figure S4D). However, under hypoxic conditions, the compensation by ACSS1 was compromised

(Figure S4D). This is in line with the observation that ACSS1 mRNA expression was downregulated during hypoxia, which is completely opposite to the mRNA regulation of ACSS2 (Figure S4E).

Subsequently, we supplied cells with $^{13}C_6$-glucose, $^{13}C_5$-glutamine, or $^{13}C_2$-acetate to compare the relative contributions of these important nutritional sources to palmitate synthesis. In normal growth conditions, glucose was the main source for fatty acid synthesis, followed closely by acetate (Figure 5H). In contrast, metabolic stress switched the preferred nutritional source to acetate and completely abrogated the contribution from glucose (Figure 5H). As previously reported, there was an increase in glutamine-labeled palmitate during hypoxic conditions (Figure 5H; Filipp et al., 2012; Metallo et al., 2012; Mullen et al., 2012; Wise et al., 2011). However, neither glucose nor glutamine, whether in normal growth conditions or low oxygen and low serum, ever labeled palmitate as extensively as acetate did during metabolic stress.

ACSS2 Silencing Inhibits Spheroid and Tumor Growth

DU145 + shNTC and DU145 + shACSS2#64 cells were cultured as spheroids in 10% or 1% serum and in the presence or absence of doxycycline. Expression of shACSS2 by doxycycline decreased ACSS2 expression and caused significant growth inhibition, which was more pronounced under low-serum conditions (Figure 6A). We had observed previously that acetate was being used to generate lipids (Figures 4 and 5). In addition, the FASN inhibitor studies and spheroid growth after ACSS2 silencing prompted us to investigate the in vivo efficacy of ACSS2 silencing on tumor growth and survival. For this we also generated a BT474c1 cell line expressing inducible shRNA targeting ACSS2 (Figure 5A). Nude mice were injected subcutaneously with DU145, MDA-MB-468, and BT474c1 cells expressing ACSS2 shRNA or a nontargeting control or empty vector. All three xenograft models displayed decreases in tumor growth when ACSS2 was silenced (Figures 6B, 6C, S5A, and S5B). Gene silencing was confirmed by immunohistochemistry or quantitative RT-PCR (qRT-PCR) (Figures 6D, S5C, and S5D). We also noted that, by the end of the xenograft studies, all mice bearing tumors depleted of ACSS2 (i.e., +DOX) were still viable, while nontreated or vector control mice exhibited higher mortality rates, which were not necessarily associated with tumor burden (Figure 6E).

Our previous results suggested that ACSS2 expression was often upregulated under hypoxic conditions (Figure 3). To examine this in vivo, serial sections from three separate BT474c1 + shACSS2#20 (no DOX) tumors were stained with pimonidazole, a hypoxia-selective marker, and ACSS2. Indeed, costaining was observed, indicating that hypoxic tumor regions have significantly higher levels of ACSS2 compared to nonhypoxic regions (Figures 6F and 6G). Together, these results confirm that ACSS2 is upregulated in areas of hypoxia in tumors and required for efficient growth and survival of cancer cells in vivo.

DISCUSSION

Hypoxia is a common feature of tumors that have a poor clinical prognosis and display aggressive traits, such as increased met-astatic and migratory potential, chemoresistance, and stemness. We also know that lipid metabolism is altered drastically under these conditions (Ackerman and Simon, 2014). Our initial studies identified that most breast and prostate cancer cell lines were sensitive to fatty acid synthesis inhibition when cultured as spheroids or grown as tumor xenografts. However, the only tissue culture condition that faithfully preserved this sensitivity was when cells were grown under metabolic stress, thus, strongly suggesting that many cancer cells find a means to survive and proliferate regardless of poor nutrient delivery and hypoxia.

The functional screens and in-vivo-induced silencing of ACSS2 in tumor xenografts highlighted the essentiality of ACSS2 under metabolically stressed conditions. The metabolic and lipidomic analyses revealed a mechanistic solution for the need of acetate and ACSS2 in cancer cells by demonstrating that, under tumor-like tissue culture conditions, there is a switch in nutrient utilization from glucose to acetate to support fatty acid and lipid biosynthesis. In support of this mechanism, we found that ACSS2 was indeed significantly upregulated in hypoxic regions of tumor xenografts and when cancer cells were exposed to prolonged oxygen and lipid withdrawal. ACSS2 expression was transcriptionally controlled by a synergistic interaction between HIF and SREBF2 signaling. In addition, copy-number gain of ACSS2 was observed in breast carcinoma, and the lack of cancer consensus genes and the size of the narrow amplicon region suggested selection pressure. The data mining information was supported by results from examining tissue microarrays showing that ACSS2 was highly expressed in IDCs, the most common histological breast cancer subtype. Likewise, increased ACSS2 expression seemed to be more closely associated with prostate metastasis than in primary tumors.

Our observed link between acetate metabolism and tumor growth coupled with the knowledge that the primary source of acetate production within the body is by the intestinal microbiota compelled us to investigate if there was a potential link between colorectal cancers and ACSS2. Further cancer data mining revealed copy-number gain or upregulation of ACSS2 in more than a quarter of all colorectal cancer (data not shown). If ACSS2 silencing proves to be effective at inhibiting colorectal tumor growth, it may reveal a disease in which ACSS2 would be an attractive target for future drug discovery. Furthermore, in cells with active lipid biosynthesis, acetate is converted to acetyl-CoA in the cytosol and then incorporated into fatty acids. Therefore, radiolabeled acetate is the most lipid-specific tracer available for positron emission tomography (PET) imaging. Acetate-based PET tracers are established clinical tools, but to date there is not enough information on how this tracer reflects perturbations in lipid biosynthesis in cancer cells (Lewis et al., 2014; Oyama et al., 2002; Yun et al., 2009). We have identified a dependency of breast cancers and prostate cancer on acetate metabolism and ACSS2 activity. This presents an attractive opportunity to use tracer technology to identify tumors that would be responsive to ACSS2-targeted therapy. Moreover, as acetate uptake is coupled to ACSS2 activity, acetate PET tracers could provide an important pharmacodynamic biomarker for treatment response and for detecting when tumors become refractory to treatment.
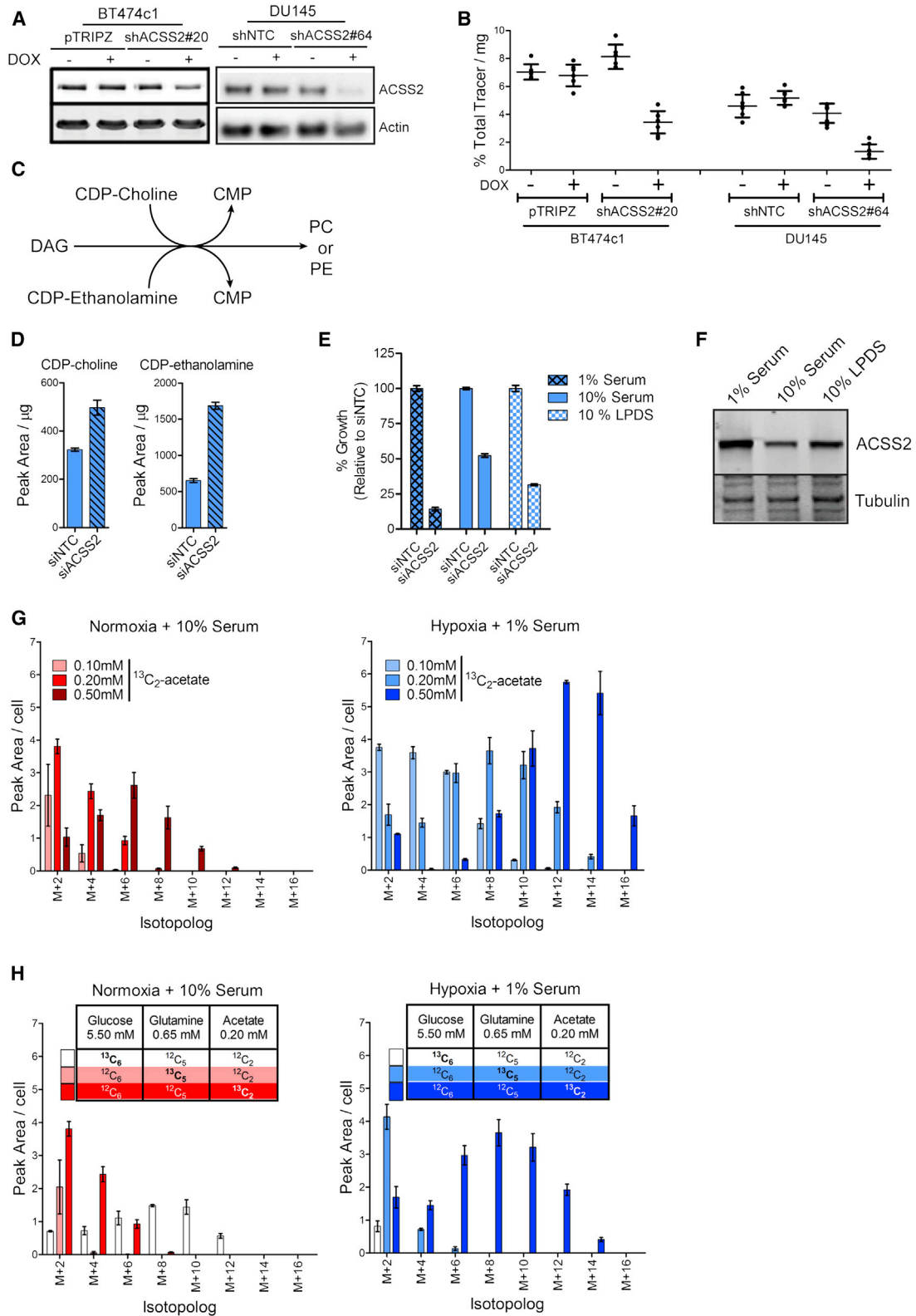
Figure 5. Acetate Is the Major Contributor to Palmitate Synthesis during Metabolic Stress

(A) Immunoblot of BT474c1 and DU145 protein extracts 72 hr postdoxycycline administration.

(B) Uptake of [³H]-acetate in BT474c1 and DU145 cells after doxycycline induced silencing of ACSS2. Cells were cultured in 10% serum and normoxia. Data are presented as mean ± SEM in triplicate (n = 2).

In conclusion, this study highlights the importance of understanding the context-dependent metabolic rewiring of cancer cells in vivo, and provides evidence that acetate is a fundamental nutrient that can fuel cancer growth. The therapeutic feasibility of pharmacologically targeting ACSS2 is currently being explored.

EXPERIMENTAL PROCEDURES

Cell Culture

LNCaP were obtained from the American Type Culture Collection. BT474c1 cells were a kind gift from Jose Baselga. All other cell lines were from the London Research Institute (CRUK) cell services. DU145, LNCaP, and PC3 cell lines were grown in RPMI supplemented with either 10% or 1% fetal calf serum (PAA Laboratories), 2 mM L-glutamine, and penicillin/streptomycin. MCF7, BT20, BT474, BT474c1, BT549, MDA-MB-231, MDA-MB-468, SkBr3, and T47D cell lines were grown in Dulbecco's modified Eagle's medium (DMEM)/F12 with either 10% or 1% fetal calf serum (PAA Laboratories), 2 mM L-glutamine, and penicillin/streptomycin. MCF10a and MCF10A + HER2 (a kind gift from Dr. Zachary Schafer) cells were grown in DMEM/F12 with either 5% or 0.5% horse serum with 20 ng/ml epidermal growth factor, 5 μg/ml hydrocortisone, 10 μg/ml insulin, and 100 ng/ml cholera toxin.

Antibodies and Reagents

ACSS2 (AceS1) antibody (D19C6) and FASN were purchased from Cell Signaling Technology. Antitubulin, antiactin, anti-ACSS1 (HPA043228), and anti-ACSS2 (HPA004141) antibodies were purchased from Sigma-Aldrich. HypoxyProbe kit, including pimonidazole, was purchased from Chemicon International. All chemicals were purchased from Fisher Scientific or Sigma-Aldrich. The ^{13}C-labeled metabolites were purchased from Cambridge Isotopes, and ^{14}C-labeled and ^{3}H-labeled acetate were purchased from PerkinElmer. Secondary antibodies were purchased from LI-COR Biosciences.

Spheroid Growth Assay

For spheroid formation, cells were trypsinized, counted, mixed with 2% matrigel in culture medium, and placed in 96-well ultralow attachment plates (Costar). Spheroid formation was initiated by centrifugation at $850 \times g$ for 10 min, and cultures were incubated for the times indicated. Fresh growth medium, containing either ethanol or doxycycline (0.5 mg/ml), was administered every 48 hr. Spheroid size was determined at the times indicated by automated imaging on an inverted microscope (Axiovert 100M, Carl Zeiss).

Xenograft Experiments

Female BALB/c nude mice (Charles River Laboratories) were injected subcutaneously with BT474, BT474c1, DU145, or MDA-MB-468 cells and allowed to establish for 1 week. When BT474 or BT474c1 cells were used, mice were implanted with 17-beta-estradiol 0.36 mg/pellet 24 hr prior to injection of cells. For shRNA induction, animals were given a doxycycline-containing diet (Harlan Laboratories) or doxycycline-supplemented drinking water, and tumor growth was followed for the indicated time period. Tumor volume was determined by caliper measurements and the

ellipsoidal volume formula: $\frac{1}{2} \times length \times width^2$. Where available, tumor burden also was determined using bioluminescence imaging at indicated times. Mice were maintained in individually ventilated cages with environmental enrichment. All procedures were performed with anesthetic and postoperative analgesics under the Animal (Scientific Procedures) Act 1986 and the EU Directive 2010. Animal experiments at Imperial College London were carried out under UK Home Office Project License 70/7177 (E.O.A.) with ethical approval from Imperial College London within a Designated Establishment under the Act (the Central Biomedical Services Unit at Imperial College London). Animal experiments at the London Research Institute were performed under UK Home Office Project License 80/2330 (A.S.) after approval by a local ethics committee. Animal experiments at the Beatson Institute were performed under UK Home Office Project License 60/4181 (K.B.) and carried out with ethical approval from University of Glasgow.

LC-MS

Cells were plated onto 12-well plates and cultured in standard medium DMEM/F12 + 10% fetal bovine serum and 2 mM glutamine. Medium was replaced for specified periods with fresh physiologically relevant medium containing amino acid concentrations as dictated by http://www.nlm.nih.gov/medlineplus/ency/article/003361.htm. In addition, all heavy carbon labeling was done using final concentrations of 5.5 mM glucose, or 0.65 mM glutamine, and 0.10–0.50 mM acetate. Metabolites were extracted with a cold solution ($-20°C$) composed of methanol, acetonitrile, and water (5:3:2). The insoluble material was immediately pelleted in a cooled (0°C) centrifuge at $16,000 \times g$ for 15 min, and the supernatant was collected for subsequent LC-MS analysis. The protein concentration in each well was calculated using a Lowry assay. Alternatively, a separate plate was seeded in parallel and used for cell counts. A ZIC-pHILIC column (4.6 × 150 mm, guard column 2.1 × 20 mm, Merck) was used for LC separation using formic acid, water, and acetonitrile as component of the mobile phase. Metabolites were detected using Thermo Exactive mass spectrometer (Thermo Fisher Scientific).

For lipidomic studies, cells were incubated in media containing 5.5 mM $^{13}C_6$-glucose for 24 hr prior to lipid isolation. Cell pellets were washed twice with cold degassed PBS and resuspended in methanol before transfer to silanized glass tubes on dry ice to Babraham Lipidomics Facility for lipid extraction and analysis. Samples were spiked with 400 ng 12:0/12:0-PC, 100 ng 17:0-LPC, 300 ng 12:0/12:0-PE, and 100 ng 17:1-LPE; 0.88% NaCl; and chloroform. The mixture was vortexed for 20 s at room temperature and sonicated in an ice-cold water bath for 2 min. Samples were centrifuged at 1,100 rpm at 4°C for 15 min. The lower phase was collected. The upper phase was extracted with synthetic lower phase (mix chloroform/methanol/0.88% NaCl at volume ratio of 2:1:1, after phase separation, take the lower phase as synthetic lower phase for second extraction of lipid). The resulting lower phase was combined and dried under vacuum at room temperature with SpeedVac (Thermo Scientific) and redissolved in chloroform. The final product was injected for LC-MS/MS analysis using a Thermo Orbitrap Elite system (Thermo Fisher Scientific) hyphenated with a five-channel online degasser, four-pump, column oven, and autosampler with cooler Prominence HPLC system (Shimadzu) for lipids analysis. In detail, lipid classes were separated on a normal-phase silica gel column (2.1 × 150 mm, 4micro, MicoSolv Technology) with hexane/dichloromethane/chloroform/methanol/acetanitrile/water/ethylamine solvent gradient based on the polarity of head group. High resolution (240k at m/z 400)/accurate mass (with mass accuracy < 5 ppm) and tandem

(C) Schematic representation of the final reaction in the synthesis of PC and PE.

(D) Change in the steady-state intracellular levels of CDP-choline and CDP-ethanolamine following transfection of the indicated siRNAs in BT474c1 cells cultured in SMEM + 1% serum and hypoxia (0.1% O_2). Data are presented as mean ± SEM (n = 3).

(E) BT474c1 cells were transfected with indicated siRNAs for 24 hr prior to the addition of 1% serum, 10% serum, or 10% LPDS and transferred to hypoxia (0.1% O_2). Cell counts were performed 72 hr later. Data are normalized to a nontargeting siRNA control for each condition and represent the mean ± SEM in triplicate (n = 1).

(F) Immunoblot for ACSS2 expression in cell lysates from the experiment in (E).

(G) $^{13}C_2$-acetate-dependent labeling of palmitate in indicated growth conditions after 24 hr. Data are presented as mean ± SEM (n = 3).

(H) $^{13}C_6$-glucose-, $^{13}C_5$-glutamine-, and $^{13}C_2$-acetate-dependent labeling of palmitate in indicated growth conditions after 24 hr. The relative concentrations of glucose, glutamine, and acetate were equal in all three conditions. Data are presented as mean ± SEM (n = 3).

See also Figure S4.
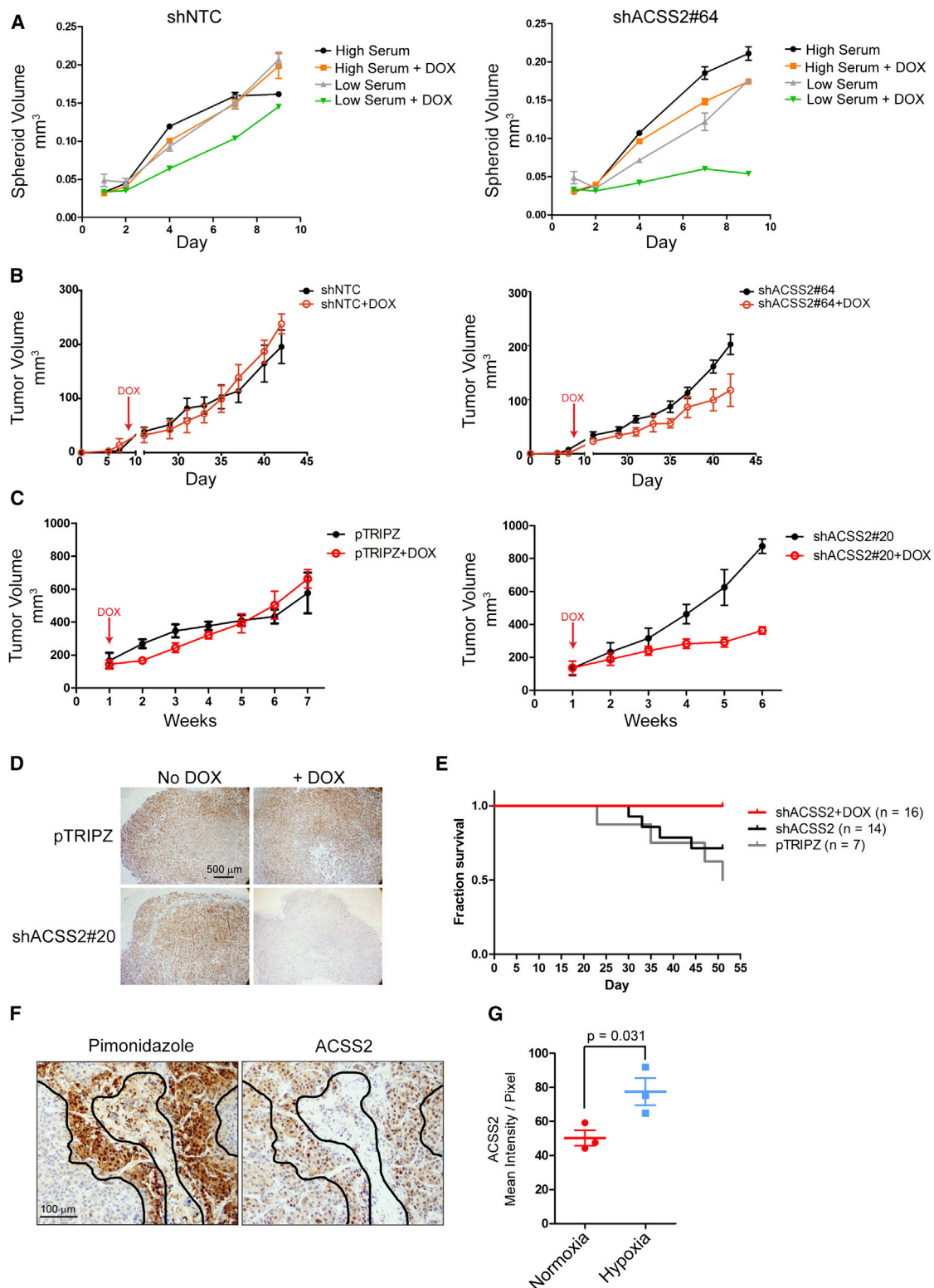
Figure 6. Silencing of ACSS2 Expression Inhibited Tumor Xenograft Growth

(A) Spheroid growth was monitored following doxycycline-induced ACSS2 silencing in DU145 + shNTC and DU145 + shACSS2#64 cells in indicated growth conditions. Data are presented as mean ± SEM (n ≥ 4).

(B and C) Nude mice (nu/nu) were injected subcutaneously with DU145 (B) or BT474c1 (C) cells. Silencing of ACSS2 was initiated by providing doxycycline at the indicated time. Each group is presented mean tumor volume ± SEM.

(legend continued on next page)

MS (collision-induced fragmentation) were used for molecular species identification and quantification. The identity of lipid was further confirmed by reference to appropriate lipids standards.

See also the Supplemental Experimental Procedures.

REFERENCES

Ackerman, D., and Simon, M.C. (2014). Hypoxia, lipids, and cancer: surviving the harsh tumor microenvironment. Trends Cell Biol. *24*, 472–478.

Alli, P.M., Pinn, M.L., Jaffee, E.M., McFadden, J.M., and Kuhajda, F.P. (2005). Fatty acid synthase inhibitors are chemopreventive for mammary cancer in neu-N transgenic mice. Oncogene *24*, 39–46.

Baenke, F., Peck, B., Miess, H., and Schulze, A. (2013). Hooked on fat: the role of lipid synthesis in cancer metabolism and tumour development. Dis. Model. Mech. *6*, 1353–1363.

Barretina, J., Caponigro, G., Stransky, N., Venkatesan, K., Margolin, A.A., Kim, S., Wilson, C.J., Lehár, J., Kryukov, G.V., Sonkin, D., et al. (2012). The Cancer Cell Line Encyclopedia enables predictive modelling of anticancer drug sensitivity. Nature *483*, 603–607.

Beckers, A., Organe, S., Timmermans, L., Scheys, K., Peeters, A., Brusselmans, K., Verhoeven, G., and Swinnen, J.V. (2007). Chemical inhibition of acetyl-CoA carboxylase induces growth arrest and cytotoxicity selectively in cancer cells. Cancer Res. *67*, 8180–8187.

Bensaad, K., Favaro, E., Lewis, C.A., Peck, B., Lord, S., Collins, J.M., Pinnick, K.E., Wigfield, S., Buffa, F.M., Li, J.L., et al. (2014). Fatty acid uptake and lipid storage induced by HIF-1α contribute to cell growth and survival after hypoxia-reoxygenation. Cell Reports *9*, 349–365.

Briggs, M.R., Yokoyama, C., Wang, X., Brown, M.S., and Goldstein, J.L. (1993). Nuclear protein that binds sterol regulatory element of low density lipoprotein receptor promoter. I. Identification of the protein and delineation of its target nucleotide sequence. J. Biol. Chem. *268*, 14490–14496.

Brinkmann, U., Gallo, M., Polymeropoulos, M.H., and Pastan, I. (1996). The human CAS (cellular apoptosis susceptibility) gene mapping on chromosome 20q13 is amplified in BT474 breast cancer cells and part of aberrant chromosomes in breast and colon cancer cell lines. Genome Res. *6*, 187–194.

Brockmöller, S.F., Bucher, E., Müller, B.M., Budczies, J., Hilvo, M., Griffin, J.L., Orešič, M., Kallioniemi, O., Iljin, K., Loibl, S., et al. (2012). Integration of metabolomics and expression of glycerol-3-phosphate acyltransferase (GPAM) in breast cancer-link to patient survival, hormone receptor status, and metabolic profiling. J. Proteome Res. *11*, 850–860.

Curtis, C., Shah, S.P., Chin, S.F., Turashvili, G., Rueda, O.M., Dunning, M.J., Speed, D., Lynch, A.G., Samarajiwa, S., Yuan, Y., et al.; METABRIC Group (2012). The genomic and transcriptomic architecture of 2,000 breast tumours reveals novel subgroups. Nature *486*, 346–352.

De Schrijver, E., Brusselmans, K., Heyns, W., Verhoeven, G., and Swinnen, J.V. (2003). RNA interference-mediated silencing of the fatty acid synthase gene attenuates growth and induces morphological changes and apoptosis of LNCaP prostate cancer cells. Cancer Res. *63*, 3799–3804.

Filipp, F.V., Scott, D.A., Ronai, Z.A., Osterman, A.L., and Smith, J.W. (2012). Reverse TCA cycle flux through isocitrate dehydrogenases 1 and 2 is required for lipogenesis in hypoxic melanoma cells. Pigment Cell Melanoma Res. *25*, 375–383.

Folger, O., Jerby, L., Frezza, C., Gottlieb, E., Ruppin, E., and Shlomi, T. (2011). Predicting selective drug targets in cancer through metabolic networks. Mol. Syst. Biol. *7*, 501.

Forbes, S.A., Bindal, N., Bamford, S., Cole, C., Kok, C.Y., Beare, D., Jia, M., Shepherd, R., Leung, K., Menzies, A., et al. (2011). COSMIC: mining complete cancer genomes in the Catalogue of Somatic Mutations in Cancer. Nucleic Acids Res. *39*, D945–D950.

Fujino, T., Kondo, J., Ishikawa, M., Morikawa, K., and Yamamoto, T.T. (2001). Acetyl-CoA synthetase 2, a mitochondrial matrix enzyme involved in the oxidation of acetate. J. Biol. Chem. *276*, 11420–11426.

Guan, X.Y., Xu, J., Anzick, S.L., Zhang, H., Trent, J.M., and Meltzer, P.S. (1996). Hybrid selection of transcribed sequences from microdissected DNA: isolation of genes within amplified region at 20q11-q13.2 in breast cancer. Cancer Res. *56*, 3446–3450.

Hatzivassiliou, G., Zhao, F., Bauer, D.E., Andreadis, C., Shaw, A.N., Dhanak, D., Hingorani, S.R., Tuveson, D.A., and Thompson, C.B. (2005). ATP citrate lyase inhibition can suppress tumor cell growth. Cancer Cell *8*, 311–321.

(D) Immunohistochemistry for ACSS2 at day 22 in BT474c1 tumors.
(E) Kaplan-Meier plot of survival of BT474c1 tumor-xenografted mice (n = total number of mice injected subcutaneously for each condition).
(F) Immunohistochemical staining of serial sections from a BT474c1 + shACSS2#20 tumors (no DOX) with antipimonidazole (hypoxia marker) and anti-ACSS2 antibodies. Hypoxic regions are outlined in black.
(G) Mean intensity of ACSS2 staining per pixel in normoxic (pimonidazole-negative) versus hypoxic (pimonidazole-positive) regions of three individual tumor sections. Data are presented as mean ± SEM (n = 3; p value = 0.031, paired, two-tailed t test).
See also Figure S5.

Hilvo, M., Denkert, C., Lehtinen, L., Müller, B., Brockmöller, S., Seppänen-Laakso, T., Budczies, J., Bucher, E., Yetukuri, L., Castillo, S., et al. (2011). Novel theranostic opportunities offered by characterization of altered membrane lipid metabolism in breast cancer progression. Cancer Res. 71, 3236–3245.

Kim, J.W., Tchernyshyov, I., Semenza, G.L., and Dang, C.V. (2006). HIF-1-mediated expression of pyruvate dehydrogenase kinase: a metabolic switch required for cellular adaptation to hypoxia. Cell Metab. 3, 177–185.

Kimura, I., Ozawa, K., Inoue, D., Imamura, T., Kimura, K., Maeda, T., Terasawa, K., Kashihara, D., Hirano, K., Tani, T., et al. (2013). The gut microbiota suppresses insulin-mediated fat accumulation via the short-chain fatty acid receptor GPR43. Nat. Commun. 4, 1829.

Kuhajda, F.P., Jenner, K., Wood, F.D., Hennigar, R.A., Jacobs, L.B., Dick, J.D., and Pasternack, G.R. (1994). Fatty acid synthesis: a potential selective target for antineoplastic therapy. Proc. Natl. Acad. Sci. USA 91, 6379–6383.

Lewis, D.Y., Boren, J., Shaw, G.L., Bielik, R., Ramos-Montoya, A., Larkin, T.J., Martins, C.P., Neal, D.E., Soloviev, D., and Brindle, K.M. (2014). Late imaging with [1-11C]acetate improves detection of tumor fatty acid synthesis with PET. J. Nucl. Med. 55, 1144–1149.

Lundquist, F., Tygstrup, N., Winkler, K., Mellemgaard, K., and Munck-Petersen, S. (1962). Ethanol metabolism and production of free acetate in the human liver. J. Clin. Invest. 41, 955–961.

Luong, A., Hannah, V.C., Brown, M.S., and Goldstein, J.L. (2000). Molecular characterization of human acetyl-CoA synthetase, an enzyme regulated by sterol regulatory element-binding proteins. J. Biol. Chem. 275, 26458–26466.

Maxwell, C.R., Spangenberg, R.J., Hoek, J.B., Silberstein, S.D., and Oshinsky, M.L. (2010). Acetate causes alcohol hangover headache in rats. PLoS ONE 5, e15963.

Menendez, J.A., and Lupu, R. (2007). Fatty acid synthase and the lipogenic phenotype in cancer pathogenesis. Nat. Rev. Cancer 7, 763–777.

Metallo, C.M., Gameiro, P.A., Bell, E.L., Mattaini, K.R., Yang, J., Hiller, K., Jewell, C.M., Johnson, Z.R., Irvine, D.J., Guarente, L., et al. (2012). Reductive glutamine metabolism by IDH1 mediates lipogenesis under hypoxia. Nature 481, 380–384.

Migita, T., Ruiz, S., Fornari, A., Fiorentino, M., Priolo, C., Zadra, G., Inazuka, F., Grisanzio, C., Palescandolo, E., Shin, E., et al. (2009). Fatty acid synthase: a metabolic enzyme and candidate oncogene in prostate cancer. J. Natl. Cancer Inst. 101, 519–532.

Mullen, A.R., Wheaton, W.W., Jin, E.S., Chen, P.H., Sullivan, L.B., Cheng, T., Yang, Y., Linehan, W.M., Chandel, N.S., and DeBerardinis, R.J. (2012). Reductive carboxylation supports growth in tumour cells with defective mitochondria. Nature 481, 385–388.

Orita, H., Coulter, J., Tully, E., Kuhajda, F.P., and Gabrielson, E. (2008). Inhibiting fatty acid synthase for chemoprevention of chemically induced lung tumors. Clin. Cancer Res. 14, 2458–2464.

Oyama, N., Akino, H., Kanamaru, H., Suzuki, Y., Muramoto, S., Yonekura, Y., Sadato, N., Yamamoto, K., and Okada, K. (2002). 11C-acetate PET imaging of prostate cancer. J. Nucl. Med. 43, 181–186.

Papandreou, I., Cairns, R.A., Fontana, L., Lim, A.L., and Denko, N.C. (2006). HIF-1 mediates adaptation to hypoxia by actively downregulating mitochondrial oxygen consumption. Cell Metab. 3, 187–197.

Pinkel, D., Segraves, R., Sudar, D., Clark, S., Poole, I., Kowbel, D., Collins, C., Kuo, W.L., Chen, C., Zhai, Y., et al. (1998). High resolution analysis of DNA copy number variation using comparative genomic hybridization to microarrays. Nat. Genet. 20, 207–211.

Pizer, E.S., Jackisch, C., Wood, F.D., Pasternack, G.R., Davidson, N.E., and Kuhajda, F.P. (1996a). Inhibition of fatty acid synthesis induces programmed cell death in human breast cancer cells. Cancer Res. 56, 2745–2747.

Pizer, E.S., Wood, F.D., Heine, H.S., Romantsev, F.E., Pasternack, G.R., and Kuhajda, F.P. (1996b). Inhibition of fatty acid synthesis delays disease progression in a xenograft model of ovarian cancer. Cancer Res. 56, 1189–1193.

Pizer, E.S., Wood, F.D., Pasternack, G.R., and Kuhajda, F.P. (1996c). Fatty acid synthase (FAS): a target for cytotoxic antimetabolites in HL60 promyelocytic leukemia cells. Cancer Res. 56, 745–751.

Pizer, E.S., Pflug, B.R., Bova, G.S., Han, W.F., Udan, M.S., and Nelson, J.B. (2001). Increased fatty acid synthase as a therapeutic target in androgen-independent prostate cancer progression. Prostate 47, 102–110.

Porstmann, T., Santos, C.R., Griffiths, B., Cully, M., Wu, M., Leevers, S., Griffiths, J.R., Chung, Y.L., and Schulze, A. (2008). SREBP activity is regulated by mTORC1 and contributes to Akt-dependent cell growth. Cell Metab. 8, 224–236.

Puig, T., Turrado, C., Benhamú, B., Aguilar, H., Relat, J., Ortega-Gutiérrez, S., Casals, G., Marrero, P.F., Urruticoechea, A., Haro, D., et al. (2009). Novel inhibitors of fatty acid synthase with anticancer activity. Clin. Cancer Res. 15, 7608–7615.

Roncari, D.A. (1974). Mammalian fatty acid synthetase. I. Purification and properties of human liver complex. Can. J. Biochem. 52, 221–230.

Roncari, D.A. (1975). Mammalian fatty acid synthetase. II. Modification of purified human liver complex activity. Can. J. Biochem. 53, 135–142.

Rondón-Lagos, M., Verdun Di Cantogno, L., Marchiò, C., Rangel, N., Payan-Gomez, C., Gugliotta, P., Botta, C., Bussolati, G., Ramírez-Clavijo, S.R., Pasini, B., and Sapino, A. (2014). Differences and homologies of chromosomal alterations within and between breast cancer cell lines: a clustering analysis. Mol. Cytogenet. 7, 8.

Rysman, E., Brusselmans, K., Scheys, K., Timmermans, L., Derua, R., Munck, S., Van Veldhoven, P.P., Waltregny, D., Daniëls, V.W., Machiels, J., et al. (2010). De novo lipogenesis protects cancer cells from free radicals and chemotherapeutics by promoting membrane lipid saturation. Cancer Res. 70, 8117–8126.

Sahar, S., Masubuchi, S., Eckel-Mahan, K., Vollmer, S., Galla, L., Ceglia, N., Masri, S., Barth, T.K., Grimaldi, B., Oluyemi, O., et al. (2014). Circadian control of fatty acid elongation by SIRT1 protein-mediated deacetylation of acetyl-co-enzyme A synthetase 1. J. Biol. Chem. 289, 6091–6097.

Scheppach, W., Pomare, E.W., Elia, M., and Cummings, J.H. (1991). The contribution of the large intestine to blood acetate in man. Clin. Sci. 80, 177–182.

Schwer, B., Bunkenborg, J., Verdin, R.O., Andersen, J.S., and Verdin, E. (2006). Reversible lysine acetylation controls the activity of the mitochondrial enzyme acetyl-CoA synthetase 2. Proc. Natl. Acad. Sci. USA 103, 10224–10229.

Shao, D.D., Tsherniak, A., Gopal, S., Weir, B.A., Tamayo, P., Stransky, N., Schumacher, S.E., Zack, T.I., Beroukhim, R., Garraway, L.A., et al. (2013). ATARiS: computational quantification of gene suppression phenotypes from multisample RNAi screens. Genome Res. 23, 665–678.

Skutches, C.L., Holroyde, C.P., Myers, R.N., Paul, P., and Reichard, G.A. (1979). Plasma acetate turnover and oxidation. J. Clin. Invest. 64, 708–713.

Sone, H., Shimano, H., Sakakura, Y., Inoue, N., Amemiya-Kudo, M., Yahagi, N., Osawa, M., Suzuki, H., Yokoo, T., Takahashi, A., et al. (2002). Acetyl-coenzyme A synthetase is a lipogenic enzyme controlled by SREBP-1 and energy status. Am. J. Physiol. Endocrinol. Metab. 282, E222–E230.

Swinnen, J.V., Heemers, H., Deboel, L., Foufelle, F., Heyns, W., and Verhoeven, G. (2000a). Stimulation of tumor-associated fatty acid synthase expression by growth factor activation of the sterol regulatory element-binding protein pathway. Oncogene 19, 5173–5181.

Swinnen, J.V., Vanderhoydonc, F., Elgamal, A.A., Eelen, M., Vercaeren, I., Joniau, S., Van Poppel, H., Baert, L., Goossens, K., Heyns, W., and Verhoeven, G. (2000b). Selective activation of the fatty acid synthesis pathway in human prostate cancer. Int. J. Cancer 88, 176–179.

Swinnen, J.V., Roskams, T., Joniau, S., Van Poppel, H., Oyen, R., Baert, L., Heyns, W., and Verhoeven, G. (2002). Overexpression of fatty acid synthase is an early and common event in the development of prostate cancer. Int. J. Cancer 98, 19–22.

Tollinger, C.D., Vreman, H.J., and Weiner, M.W. (1979). Measurement of acetate in human blood by gas chromatography: effects of sample preparation, feeding, and various diseases. Clin. Chem. 25, 1787–1790.

Tsukamoto, S., Muto, T., Nagoya, T., Shimamura, M., Saito, M., and Tainaka, H. (1989). Determinations of ethanol, acetaldehyde and acetate in blood and urine during alcohol oxidation in man. Alcohol Alcohol. 24, 101–108.

Tucek, S. (1967). Subcellular distribution of acetyl-CoA synthetase, ATP citrate lyase, citrate synthase, choline acetyltransferase, fumarate hydratase and lactate dehydrogenase in mammalian brain tissue. J. Neurochem. *14*, 531–545.

Vaapil, M., Helczynska, K., Villadsen, R., Petersen, O.W., Johansson, E., Beckman, S., Larsson, C., Påhlman, S., and Jögi, A. (2012). Hypoxic conditions induce a cancer-like phenotype in human breast epithelial cells. PLoS ONE *7*, e46543.

Wang, X., Briggs, M.R., Hua, X., Yokoyama, C., Goldstein, J.L., and Brown, M.S. (1993). Nuclear protein that binds sterol regulatory element of low density lipoprotein receptor promoter. II. Purification and characterization. J. Biol. Chem. *268*, 14497–14504.

Watkins, P.A., Maiguel, D., Jia, Z., and Pevsner, J. (2007). Evidence for 26 distinct acyl-coenzyme A synthetase genes in the human genome. J. Lipid Res. *48*, 2736–2750.

Watson, J.A., Watson, C.J., McCrohan, A.M., Woodfine, K., Tosetto, M., McDaid, J., Gallagher, E., Betts, D., Baugh, J., O'Sullivan, J., et al. (2009). Generation of an epigenetic signature by chronic hypoxia in prostate cells. Hum. Mol. Genet. *18*, 3594–3604.

Wise, D.R., Ward, P.S., Shay, J.E., Cross, J.R., Gruber, J.J., Sachdeva, U.M., Platt, J.M., DeMatteo, R.G., Simon, M.C., and Thompson, C.B. (2011). Hypoxia promotes isocitrate dehydrogenase-dependent carboxylation of α-ketoglutarate to citrate to support cell growth and viability. Proc. Natl. Acad. Sci. USA *108*, 19611–19616.

Yoshii, Y., Furukawa, T., Yoshii, H., Mori, T., Kiyono, Y., Waki, A., Kobayashi, M., Tsujikawa, T., Kudo, T., Okazawa, H., et al. (2009a). Cytosolic acetyl-CoA

synthetase affected tumor cell survival under hypoxia: the possible function in tumor acetyl-CoA/acetate metabolism. Cancer Sci. *100*, 821–827.

Yoshii, Y., Waki, A., Furukawa, T., Kiyono, Y., Mori, T., Yoshii, H., Kudo, T., Okazawa, H., Welch, M.J., and Fujibayashi, Y. (2009b). Tumor uptake of radio-labeled acetate reflects the expression of cytosolic acetyl-CoA synthetase: implications for the mechanism of acetate PET. Nucl. Med. Biol. *36*, 771–777.

Yoshimoto, M., Waki, A., Yonekura, Y., Sadato, N., Murata, T., Omata, N., Takahashi, N., Welch, M.J., and Fujibayashi, Y. (2001). Characterization of acetate metabolism in tumor cells in relation to cell proliferation: acetate metabolism in tumor cells. Nucl. Med. Biol. *28*, 117–122.

Yun, M., Bang, S.H., Kim, J.W., Park, J.Y., Kim, K.S., and Lee, J.D. (2009). The importance of acetyl coenzyme A synthetase for 11C-acetate uptake and cell survival in hepatocellular carcinoma. J. Nucl. Med. *50*, 1222–1228.

Zaidi, N., Lupien, L., Kuemmerle, N.B., Kinlaw, W.B., Swinnen, J.V., and Smans, K. (2013). Lipogenesis and lipolysis: the pathways exploited by the cancer cells to acquire fatty acids. Prog. Lipid Res. *52*, 585–589.

Zhan, Y., Ginanni, N., Tota, M.R., Wu, M., Bays, N.W., Richon, V.M., Kohl, N.E., Bachman, E.S., Strack, P.R., and Krauss, S. (2008). Control of cell growth and survival by enzymes of the fatty acid synthesis pathway in HCT-116 colon cancer cells. Clin. Cancer Res. *14*, 5735–5742.

Zhang, X.D. (2011). Illustration of SSMD, z score, SSMD*, z* score, and t statistic for hit selection in RNAi high-throughput screens. J. Biomol. Screen. *16*, 775–785.

Zu, X.Y., Zhang, Q.H., Liu, J.H., Cao, R.X., Zhong, J., Yi, G.H., Quan, Z.H., and Pizzorno, G. (2012). ATP citrate lyase inhibitors as novel cancer therapeutic agents. Recent Patents Anticancer. Drug Discov. *7*, 154–167.